Aerosol Science and Technology

ISSN: 0278-6826 (Print) 1521-7388 (Online) Journal homepage: www.tandfonline.com/journals/uast20

Development and experimental validation of a new cleaning model to predict the removal efficiency of 10–130 nm contaminant particles on Si wafers using sprayed microdroplets: Emphasis on optimizing cleaning time

Seungwook Lee, Jeonggeon Kim & Donggeun Lee

To cite this article: Seungwook Lee, Jeonggeon Kim & Donggeun Lee (2025) Development and experimental validation of a new cleaning model to predict the removal efficiency of 10–130 nm contaminant particles on Si wafers using sprayed microdroplets: Emphasis on optimizing cleaning time, Aerosol Science and Technology, 59:6, 765-778, DOI: 10.1080/02786826.2025.2449666

To link to this article: https://doi.org/10.1080/02786826.2025.2449666

AEROSOL SCIENCE AND TECHNOLOGY
2025, VOL. 59, NO. 6, 765–778
https://doi.org/10.1080/02786826.2025.2449666

Development and experimental validation of a new cleaning model to predict the removal efficiency of 10–130 nm contaminant particles on Si wafers using sprayed microdroplets: Emphasis on optimizing cleaning time

Seungwook Lee, Jeonggeon Kim, and Donggeun Lee

School of Mechanical Engineering, Pusan National University, Busan, South Korea

ABSTRACT

Liquid jet spray cleaning has recently emerged as a promising method for removing nanoparticle contaminants from Si wafers in the semiconductor industry. However, its environmental benefits from not using chemicals are not fully realized due to limitations in the size of removable particles and insufficient removal efficiency for smaller particles. In this study, we aimed to overcome the technical limitations. We developed a Monte Carlo model that connects existing single droplet-based cleaning models to multiple droplet impacts in real cleaning experiments, enabling the prediction of removal efficiency of particles by their size. For experimental validation, we developed a water-spray cleaning system using a two-fluid supersonic nozzle capable of spraying microdroplets 10–40 μm in diameter with controlled impact velocity ranging from 14 to 100 m/s onto a wafer surface. As a result, we demonstrated for the first time that the cleaning (or spraying) time is a key parameter in determining particle removal efficiency across a size range of 10–130 nm, alongside droplet size and impact velocity. Based on this finding, we proposed a new approach to maximize the removal efficiency particularly for 10–30 nm particles, by optimizing the cleaning time to maintain a dry surface. Our Monte Carlo model reasonably predicted the size-resolved particle removal efficiency across all cases considered.

GRAPHICAL ABSTRACT

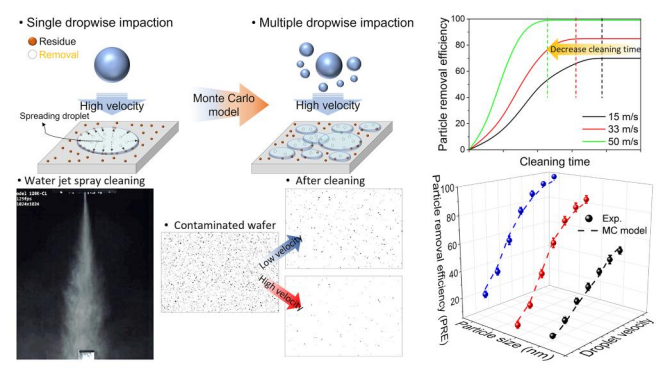

ARTICLE HISTORY
Received 2 September 2024
Accepted 21 December 2024

EDITOR
Se-Jin Yook

1. Introduction

The fabrication processes for advanced semiconductor devices are typically categorized into three key stages: Front End of Line (FEOL), Middle of Line (MOL), and Back End of Line (BEOL). A significant portion, approximately 20–25%, of these processes is related to cleaning procedures (Reinhardt and Kern 2018; Snow, Sato, and Tanaka 2013). For instance, processes such as chemical-mechanical planarization (CMP) or etching can leave behind a significant number of particulate contaminants (Hong et al. 2016). Particularly when these particles become attached to patterned wafers, they can degrade the electrical properties of semiconductor devices, leading to a reduction in their yield (Liu et al. 1996; Kim et al. 2009; Eranna 2014). This motivated the development of methods for

CONTACT Donggeun Lee donglee@pusan.ac.kr School Of Mechanical Engineering, Pusan National University, 30 Jangjeon-dong Geumjeong-gu, Kumjeong-ku, Busan 46241, South Korea.

Supplemental data for this article can be accessed online at https://doi.org/10.1080/02786826.2025.2449666.

eliminating these contaminants, which can be primarily divided into chemical cleaning methods and physical cleaning methods (Kern 1990).

Chemical cleaning, which involves using a solution mixture of hydrogen peroxide and acidic chemicals, has been employed to remove contaminants from wafer surfaces. However, the acidic chemicals can induce surface roughening through etching, which may adversely affect device performance (Ohmi et al. 1992). Furthermore, chemical cleaning requires substantial amounts of ultra-pure water and various chemicals, raising environmental and economic concerns related to waste discharge and treatment (Hattori et al. 2007).

Physical cleaning methods, on the other hand, are gaining increased attention because they utilize external forces to physically remove contaminant particles without the need for any chemical agents. These methods include brush scrubbers, cryogenic aerosol-based sprays, and liquid jet sprays (Toscano and Ahmadi 2003; Huang et al. 2011; Liu and Liu 2011; Lee et al. 2019). The brush scrubber method effectively removes slurry residues and other contaminants following the CMP process. However, it is not directly applicable to patterned wafers and may cause secondary contamination due to abrasive particles remaining in the brush (Zantye, Kumar, and Sikder 2004). Cryogenic aerosol cleaning method involves spraying tiny solid/liquid particles formed through the free expansion cooling of inert gas, typically at extremely low temperatures, to remove contaminant particles from wafer surfaces (Banerjee and Campbell 2005). In addition to its economic challenges in maintaining cryogenic temperatures, this method can induce thermal stress in patterned wafer, potentially leading to cracking or other types of damage (Huang et al. 2011).

In light of the aforementioned limitations, the liquid jet spray method emerges as a promising alternative capable of achieving effective cleaning with minimal damage to the wafers. We have summarized existing experimental studies utilizing the liquid jet spray for nanoparticle removal comparatively in Table 1. Referring to the table, early studies commonly used chemical solutions including ammonia peroxide mixture (APM) and/or hydrofluoric acid (HF) to remove sub-100 nm particles (Eitoku et al. 2003; Hirota et al. 2005; Hirano et al. 2006; Xu et al. 2009). These studies mostly reported relatively high particle removal efficiencies (PRE) ranging from 60 to 90%, with the exception of Hirano et al. (2006). Specifically, Xu et al. (2009) demonstrated that using an APM solution is more effective in removing Si_3N_4 particles (>65 nm) compared to DI water, resulting in a higher PRE of 90% versus 60%. However, subsequent research appeared to revert to spraying pure water presumably due to the environmental concern of chemicals, even though there was a decline in PRE to 35–63% for particles of comparable sizes (Watanabe et al. 2009; Sato et al. 2011; Iwasaki et al. 2015). Following Seike et al. (2010), Teng et al. (2016) reported that a notably high PRE of 90% could be achieved for particles larger than 100 nm, solely with pure water spray. However, it is noted that their methods may be questioned when targeting sub-100 nm particles, as it is more challenging to remove smaller particles (Park et al. 2024; Snow, Sato, and Tanaka 2013; Sato et al. 2011).

According to the IRDS (Institute of Electrical and Electronics Engineers 2023), the target particle size for removal has steadily decreased to below 10 nm, in line with the ongoing miniaturization of the semiconductor devices. Nevertheless, there is currently no experimental evidence supporting the efficacy of existing liquid jet spray cleaning methods (as shown in Table 1) for the removal of small particles sized between 10 to 40 nm. Furthermore, Table 1 indicates

Table 1. Previous experimental studies on particle removal *via* liquid jet spray methods, comparatively summarized in terms of detailing the kinds of gas and liquid in nozzles, droplet sizes and velocities, target particle sizes and materials, and particle removal efficiency (PRE).

Reference	Liquid	Gas	Cleaning time	Droplet size (μm)	Droplet vel. (m/s)	PRE (%)	Particle size (nm)	Particle material
Eitoku et al. (2003)	DIW, APM	N_2	–	–	–	84	> 80	PSL
Hirota et al. (2005)	DIW, APM[a]	Air or N_2	–	dozens of micron size	70	60	> 65	SiO_2
Hirano et al. (2006)	DIW, HF[b], APM	N_2	600 s			35	> 50	Si_3N_4
Xu et al. (2009)	DIW, APM	N_2	–	5–30	35–85	90	> 65	Si_3N_4
Watanabe et al. (2009)	DIW	Steam	–	20	200	63	> 87	Latex
Seike et al. (2010)	UPW[c]	Air	300 s	5–35	40–90	90	> 200	PSL
Sato et al. (2011)	DIW	N_2	–	22,40	20–80	35	> 78	SiO_2
Iwasaki et al. (2015)	DIW	N_2	–	2–38	40–100	50	> 45	Si_3N_4
Teng et al. (2016)	UPW	N_2	–	–	–	90	> 100	PSL

[a]APM: Ammonia peroxide mixture.
[b]HF: Hydrofluoric acid.
[c]UPW: Ultra-pure water.

that only two previous studies have specified the cleaning time during which a liquid solution was continuously sprayed onto the wafers for particle removal. Prolonged cleaning times inevitably result in multiple droplet impacts, leading to significant overlap between droplets and the formation of a thick liquid film on the wafer surface. According to Kondo and Ando (2019), once a liquid film forms, subsequent droplet impacts become significantly less effective in removing particles compared to a dry surface, due to the cushioning effect. Conversely, when the cleaning time is too short to result in liquid flooding, particles, after being detached from the surface, are found to not be completely removed but rather to resettle on the surface (Park et al. 2024). These two extremes may suggest that there is room for optimization of the cleaning time. However, guidance on this matter has not yet been provided.

Most recently, we proposed an effective cleaning diameter that defines the intrinsic cleaning area predicted from a single droplet impact and provided a contour plot for predicting the effective cleaning diameter based on the impaction conditions (size and velocity) of droplets (Park et al. 2024). However, this effective cleaning diameter cannot be directly used to predict the particle removal efficiency (PRE) in real experiments because it essentially represents the impact of a single droplet on a dry surface. Indeed, no model currently exists that links such a single-droplet effect to the ensemble effect arising from the multiple impacts of droplets (Zoeteweij, van der Donck, and Versluis 2009; Seike et al. 2010; Iwasaki et al. 2015; Park et al. 2024).

Hence, this study was designed to optimize the cleaning time for contaminant particles with an average size of 20 nm by bridging the gap between the cleaning models and actual cleaning experiments. To achieve this objective, we developed a supersonic two-fluid nozzle system to spray microdroplets onto a contaminated silicon wafer while controlling their impact velocities. By measuring the diameter and velocity of individual droplets, we established a database correlating the impaction conditions with effective cleaning diameters. We then developed a Monte Carlo model (Kim, Shin, and Lee 2022; Kim and Lee 2023) to simulate the spatially random impaction of size-polydisperse droplets. Concurrently, we conducted a series of experiments to provide comprehensive experimental datasets for comparison with model predictions, including size-resolved particle removal efficiencies (PREs) for particles ranging from 10 to 130 nm. Finally, we introduced a new concept to optimize the cleaning time and thereby increase PREs, based on the observed time-dependent variations of PREs with particle sizes.

2. Methods

2.1. Prediction of effective cleaning diameter (D_R) of a single droplet

In this section, we provide an overview of the effective cleaning diameter as described in our previous study (Park et al. 2024), for the readers' convenience. When a droplet impacts a dry wafer surface, it deforms into a liquid film and spreads radially, gradually decelerating due to the friction with the surface and the droplet's limited volume. The spreading ceases once it reaches the maximum diameter, D_{max}. As the liquid flows over a particle adhered to the surface (refer to Figure 1), it can generate various forces on the particle: a drag force (F_D), a lift force (F_L), and a rotational moment induced by surface stress (M_D) (Burdick, Berman, and Beaudoin 2001; Leite et al. 2012; Kondo and Ando 2019; Tran-Cong, Gay, and Michaelides 2004). Among these forces, the rolling moment induced by the drag force and the surface stress ($M_D + \frac{1}{2}F_D d_p$) is recognized as the driving force for detaching a particle with a diameter (d_p) from the surface (Burdick, Berman, and Beaudoin 2001). Conversely, the adhesion force (F_{ad}) acts as a resistance in the opposite direction.

Therefore, we employ a moment inequality $\sum M = M_D + \frac{1}{2}F_D d_p - F_{ad}a > 0$ as a criterion for judging particle detachment from the surface. Through computational fluid dynamics (CFD) simulations, we obtained

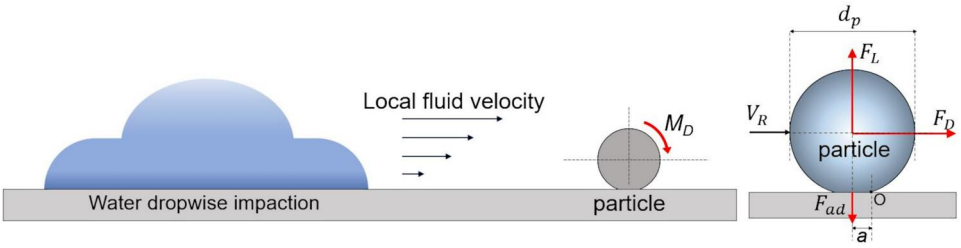

Figure 1. Dropwise impaction and its resulting forces acting on a particle adhered to a wafer surface.

the velocity field within the spreading liquid film at various positions and times, with a focus on the local velocity (V_R) at the particle center. Subsequently, we continuously monitor the size of the region where $\sum M > 0$ until the spreading ceases. The maximum size of the region determined through this process represents the effective cleaning diameter (D_R) resulting from a single droplet impact.

Following the detailed procedure outlined by Park et al. (2024), we iteratively calculate the values of D_R resulting from each impact of single droplets with various diameters at different velocities. Figure 2a presents a three-dimensional scatter plot of D_R against droplet's diameter and impact velocity, focusing on the removal of 20-nm particles. As the droplet diameter increases while maintaining a constant velocity of 10 m/s, there is a gradual but slight increase in D_R. However, at higher velocities, such as 50 m/s, the droplet diameter exhibits a more pronounced effect on particle removal, leading to a steeper, linear-like increase in D_R. In comparison, Figure 2b demonstrates that the droplet diameter is a more influential factor for the removal of 60-nm particles, particularly at a low velocity of 10 m/s, doubling the D_R compared to the case of 20-nm particles.

Upon comparing Figures 2a and b, it is evident that the D_R is influenced not only by droplet's diameter (D_0) and velocity (U) but also by the target particle diameter. This suggests a functional relationship of $D_R = f(D_0, U, d_p)$. Continuing the calculation of D_R for other diameters of target particles, we establish a comprehensive database correlating the output D_R to the three independent parameters within the range of $10\,\mu\text{m} \leq D_0 \leq 40\,\mu\text{m}$, $10\,\text{m/s} \leq U \leq 50\,\text{m/s}$, and $10\,\text{nm} \leq d_p \leq 130\,\text{nm}$. According to Park et al. (2024), there are other parameters affecting D_R, such as Hamaker constant, Young's moduli of particle and surface, and the work of adhesion at the particle-surface interface. These additional parameters are incorporated into the moment inequality as part of the adhesion force (F_{ad}) term and thus used for calculation of D_R. However, since titanium particles deposited on silicon wafers are consistently used to validate the current Model, these parameters remain constant throughout this study. This explains why the material properties are not explicitly included in the functional relationship.

Readers may find it more convenient to utilize a simple mathematical expression rather than the discrete database itself. Therefore, we further apply the rational Taylor model with the Levenberg-Marquardt algorithm (Ji et al. 2022) to the database to obtain the best-fitted rational function of $f(D_0, U, d_p)$ as follows:

$$D_R = f(D_0, U, d_p) = \frac{C_t}{C_p} = \frac{z_0 + A_{01}D_0 + B_{01}U + B_{02}U^2 + C_{02}D_0U}{1 + A_1D_0 + A_2D_0^2 + B_1U + B_2U^2 + C_2D_0U} \quad (1)$$

where z_0, A_{01}, B_{01}, B_{02}, C_{02}, A_1, A_2, B_1, B_2, and C_2 are the fitting parameters. In Equation (1), D_0 and D_R have units of micrometers, while d_p has units of nanometers.

From a preliminary test, we observe that the fitting is not very satisfactory with a single set of the parameters. Thus, we divide the range of particle diameter into three parts: $10\,\text{nm} \leq d_p \leq 60\,\text{nm}$, $60\,\text{nm} \leq d_p \leq 90\,\text{nm}$, and $d_p \geq 90\,\text{nm}$, and obtain a separate set of the fitting parameters for each range as listed in Table 2. In Figure 2, we also plot the values of D_R predicted by Equation (1) in blue for comparison with the original data in red. The model predictions are

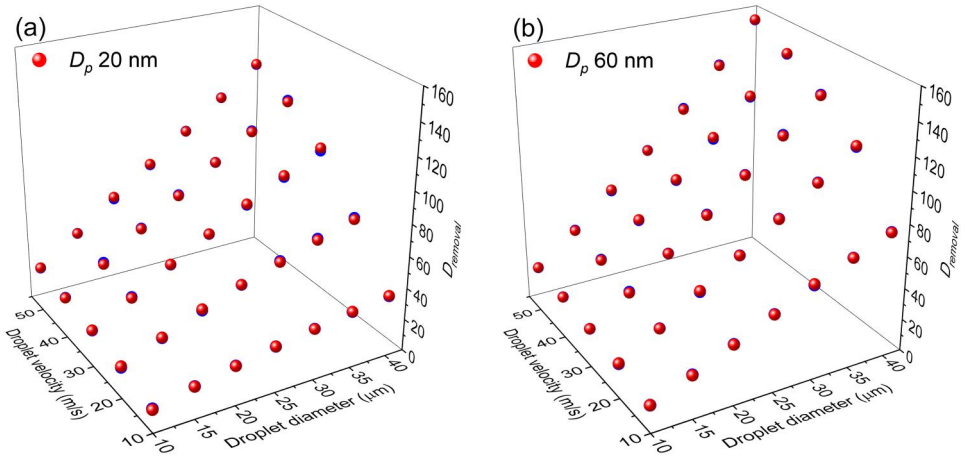

Figure 2. Variations of effective cleaning diameters of droplets with changes in droplet diameter and impact velocity, for the removal of (a) 20-nm and (b) 60-nm particles.

Table 2. Three sets of fitting parameters of the rational Taylor function obtained for the three ranges of particle diameters.

d_p (nm)	z_0	A_{01}	B_{01}	B_{02}	C_{02}	A_1	A_2	B_1	B_2	C_2
10 ~ 60	13.2648	−0.0873	−1.2088	0.0141	0.1757	0.0186	6.25×10^{-5}	0.0082	5.10×10^{-4}	-4.68×10^{-4}
60 ~ 90	13.2648	−1.7164	−1.9213	0.0116	0.7005	−0.0182	5.00×10^{-4}	0.2088	-3.72×10^{-4}	−0.0012
> 90	13.2648	−0.6213	−1.6567	0.0106	0.4424	−0.0157	1.97×10^{-4}	0.1166	-1.70×10^{-4}	-5.03×10^{-4}

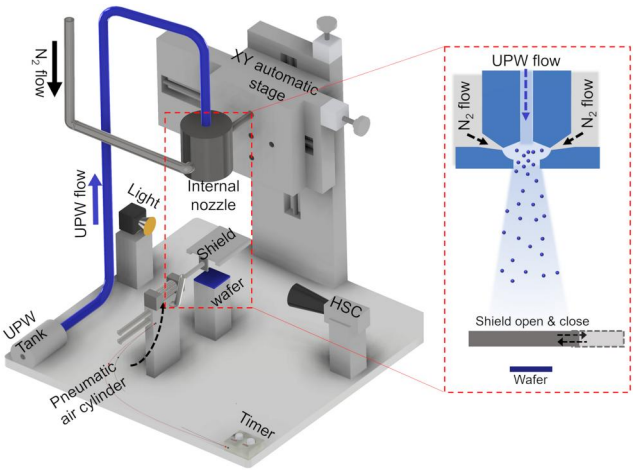

Figure 3. Experimental setup for the liquid jet spray system for cleaning the contaminated Si wafer.

notably successful across the entire range of interest, with errors within a maximum of 4%.

2.2. Experimental for nanoparticle removal from a Si wafer surface

Figure 3 illustrates a schematic diagram of our liquid jet spray system, mainly comprising a two-fluid supersonic internal-mixing nozzle, a shield plate reciprocating by a pneumatic gas cylinder, and a contaminated wafer. The nozzle was designed for nitrogen gas to strongly recirculate inside the cavity of the nozzle after being accelerated through nozzle throat, resulting in impetuous breakups of ultrapure water (UPW) before exiting the nozzle. Thus, water droplets, primarily forming inside the nozzle, were injected through the nozzle exit by the N_2 gas jet. The nozzle was installed on a motorized XY stage (SM1-0810-3S, Sciencetown Co., Korea) to adjust the nozzle exit-to-wafer distance (h) from 50 to 150 mm with a vertical resolution of 2 µm. The shield plate (5 cm × 5 cm) was horizontally positioned 5 cm away from the wafer surface and moved back and forth by a pneumatic gas cylinder equipped with a timer to control the cleaning time from 1 to 3 s with a resolution of 0.1 s.

A set of contaminated wafer samples was prepared by depositing Ti nanoparticles with an average diameter of ~20 nm, generated by a spark discharger (Lee et al. 2011; Park et al. 2024), onto a 1 cm x 1 cm silicon wafer for 30 s. These nanoparticles were positively charged using a corona discharger (Ock et al. 2018) and then electrostatically deposited onto the wafer by employing a negative voltage (5 kV) to the bottom of the wafer. A field-emission scanning electron microscope (FE-SEM; ZEISS Supra25) was used to visualize residual particles on the wafer surface. To ensure comprehensive image analysis of the entire wafer surface, we randomly selected 15 different sites on the surface, both before and after cleaning, and captured SEM images with an equal magnification ratio. We then used an open-source software ImageJ to analyze the images and measure the sizes of existing particles (Castanet et al. 2013). As an example, one of the 15 SEM images before cleaning, captured at a high magnification of 100,000x, is presented in Figure S1(a). As a result, most particles appear non-agglomerated when $d_p \leq 60$ nm, while agglomeration tends to occur in particles larger than 60 nm. To quantify this, we counted the number of agglomerated particles (i.e., those larger than 60 nm) and compared them to non-agglomerated particles. The result indicates that agglomerated particles are relatively rare, comprising only 14% of the total particle count. Additionally, we compared the size distributions of particles from five different sites on the surface, as shown in Figure S1(b), confirming a spatially uniform distribution of particles across the wafer surface. It should be noted that this procedure was consistently applied to the cases after cleaning.

To operate the nozzle, we varied the volume flow rate of ultrapure water (Q_l) in a range of 10–80 ccm while maintaining the volume flow rate of nitrogen gas (Q_g) at a constant 50 lpm. We captured the sprayed water droplets by placing a petri dish with a diameter of 3 cm containing organic liquid (1-methylnaphthalene) 20 cm away from the nozzle, ensuring that droplet impacts did not result in any splash of the organic liquid (Eigel and Moore 1983). According to the manufacturer (Sigma Aldrich), the density of the organic liquid is 1,001 kg/m^3, which is almost identical to that of water. This allows fine water droplets to remain well suspended after their impact with the organic liquid, without either floating or sinking. We visualized the captured droplets using an optical microscope (Leica, DM750M), as demonstrated in Figure S2, for subsequent image analysis using ImageJ. Figure 4a shows the size distributions of droplets

sprayed with different volume flow rates of water. Since smaller droplets are advantageous for more *efficient* removal of particles (refer to Figure 7 in Park et al. (2024)), we hereafter maintained the volume flow rate of water at 10 ccm, producing the smallest droplets with an average diameter ($\overline{D}_0$) of 23.4 µm and a standard deviation of 8.4 µm.

A high-speed camera (HSC) (Phantom, mini UX-50), combined with a LED light (40,000 lx) on the opposite side (Choudhury et al. 2017), was installed to illuminate directly above the wafer (see Figure 3) and measure the velocities (U) of individual droplets by continually tracking them (refer to Figure S3a). For this purpose, we adjusted the camera's frame rate to 100,000 FPS with an image resolution of 1280×24 pixels. We tracked 100 droplets at a specific distance from the nozzle, and then continued to measure the droplet velocity while increasing the distance from 50 to 150 mm. Figure 4b shows that the average velocity of droplets consistently decreases with the distance (h); specifically, 100 ± 9.8 m/s at $h = 50$ mm, 50 ± 3.4 m/s at $h = 100$ mm, and 14 ± 2.8 m/s at $h = 150$ mm. Additionally, the overall spray pattern was recorded with the camera operating at 250 FPS and a resolution of 1284×1024 pixels. Analysis of the video snapshots, such as in Figure S3b, revealed that the spray angle (θ) was ~27° under the spray condition of $Q_g = 50$ lpm and $Q_l = 10$ ccm.

The high-speed camera was also used to selectively monitor the gradual accumulation of droplets on the wafer surface upon impact, thereby identifying the time required for the formation of a liquid film on it. Figure 5 shows the sequential images of wafer surface taken at $h = 150$ mm (corresponding to $U = 14$ m/s from Figure 4b), starting from the initial impact of droplets. At 0.5 s, the surface appeared to be covered

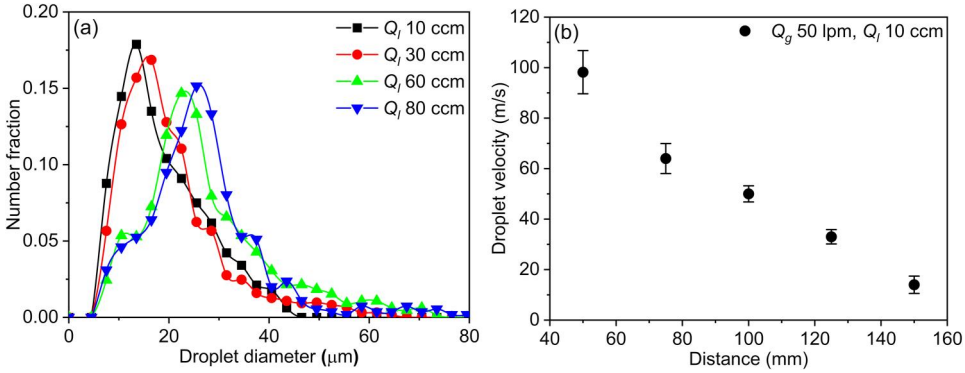

Figure 4. Spray characteristics of the current two-fluid internal-mixing nozzle: (a) size distributions of droplets obtained by the immersion method, and (b) variations of droplet's average velocity with the distance from the nozzle obtained from high-speed camera observations.

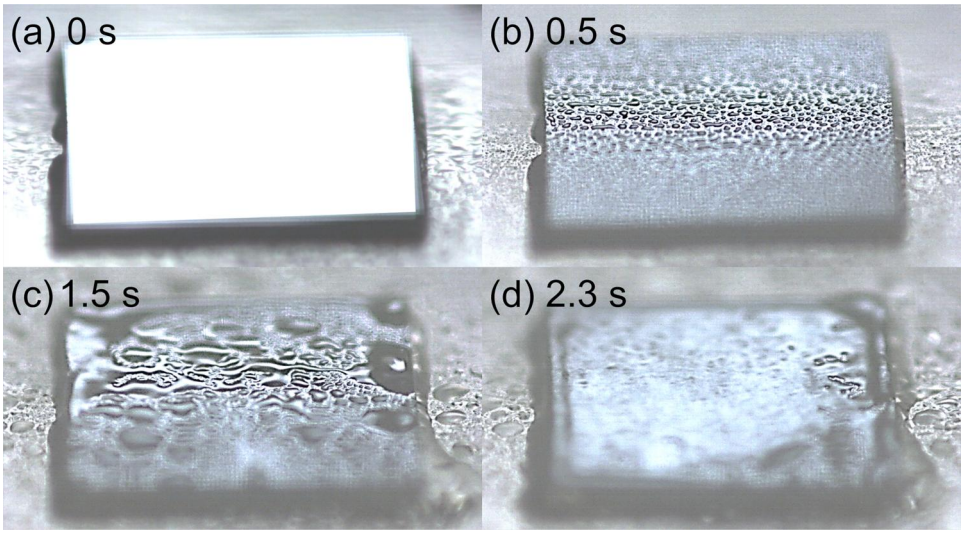

Figure 5. Sequential snapshots of wafer surface from individual droplet deposition to liquid film formation, taken at different time intervals of (a) 0 s, (b) 0.5 s, (c) 1.5 s, and (d) 2.3 s for droplet impact at $U = 14$ m/s.

with individual droplets. At 1.5 s, however, water droplets significantly coalesced to form much larger liquid drops on the surface. At 2.3 s, the surface was fully covered with a continuous water film, and the water began to flow outward from the wafer surface. Referring to the snapshots taken at different impact velocities in Figure S4, we confirmed that the time for the water film formation (τ_{film}) was shortened to 1.3 s, as expected, at an impact velocity of $U = 33$ m/s, and to 0.4 s at $U = 50$ m/s. Furthermore, we determined the thickness of water film (h_{film}) by measuring the difference in mass (Δm) of the wafer before and after droplet impacts for a duration 3 s ($> \tau_{film}$) as $h_{film} = \Delta m/(\rho_l A_{wafer})$. We found that the mass of the remaining water film Δm was invariant around 0.5 ± 0.03 mg, regardless of the droplet velocity, resulting in $h_{film} = 50 \pm 0.3$ μm.

When a wafer surface cleaned in this manner (particularly spraying an HF aqueous solution) is left to air-dry, circular water marks are often created. According to Kurumoto, Eitoku, and Miya (2009), pure isopropanol, with its low surface tension of 21.7 mN/m, can effectively prevent the water mark formation on the wafer surface by displacing residual water before evaporation. In this study, therefore, cleaned wafer samples were immersed in isopropanol (99.9%, Sigma Aldrich) for 30 s and then dried in a vacuum oven at 80 °C for 10 min, prior to SEM imaging.

2.3. Monte Carlo model for predicting particle removal efficiency

As mentioned in the Introduction, there is a discrepancy between the effective cleaning diameter of a single droplet and the particle removal efficiency resulting from multiple droplet impacts. In this study, we developed a Monte Carlo (MC) model to account for the ensemble effect of multiple droplet impacts, building upon the single-droplet performance.

To simulate multiple droplet impacts, we randomly generated droplets just above the wafer surface, covering a 1 cm x 1 cm area, and sequentially moved them to impact the surface. For this simulation, the droplets were sampled to have various diameters in accordance with the size distributions obtained from experiments, while their impact velocities were simplified to the average values measured at different distances from the nozzle during the experiments (refer to Figure 4). For each impact, the effective cleaning diameter (D_R) and maximum spreading diameter (D_{max}) were calculated by applying the impact condition to Equation (1) and using Yonemoto and Kunugi's (YK) model, respectively. Here, the YK model is the most recent analytical model to examine the relationship between a droplet's ultimate spreading and impact conditions in dimensionless form (refer to Equation (10) in Park et al. (2024)).

Figures 6a–c illustrate the circular traces left by the sequential impacts of five different droplets, characterized by their respective D_R and D_{max} values, and describe how to treat contaminant particles in response to the droplet impacts. As shown by the white circle in Figure 6a, particles initially located within $r \leq D_R/2$ were modeled to be completely removed from the surface. In the annular region ($D_R/2 \leq r \leq D_{max}/2$), denoted as '$A_{remain}$', existing particles were assumed to remain unaffected by liquid spreading toward D_{max} or even by any subsequent droplet impacts. For instance, even if another droplet with a diameter of D_2 impacts part of the circular trace of the first droplet, particles in the overlapped

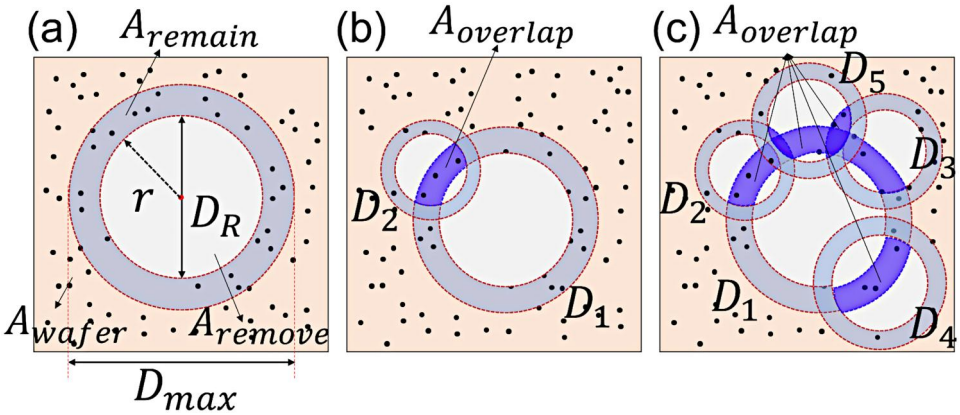

Figure 6. Schematic diagrams illustrating how to model the particle removal (a) upon impact of the first droplet with a diameter of D_1, (b) upon impact of the second droplet with D_2, and (c) during subsequent multiple droplet impacts. Tiny black dots represent contaminant particles adhered to the wafer surface, while the white area indicates the clean area obtained after particle removal.

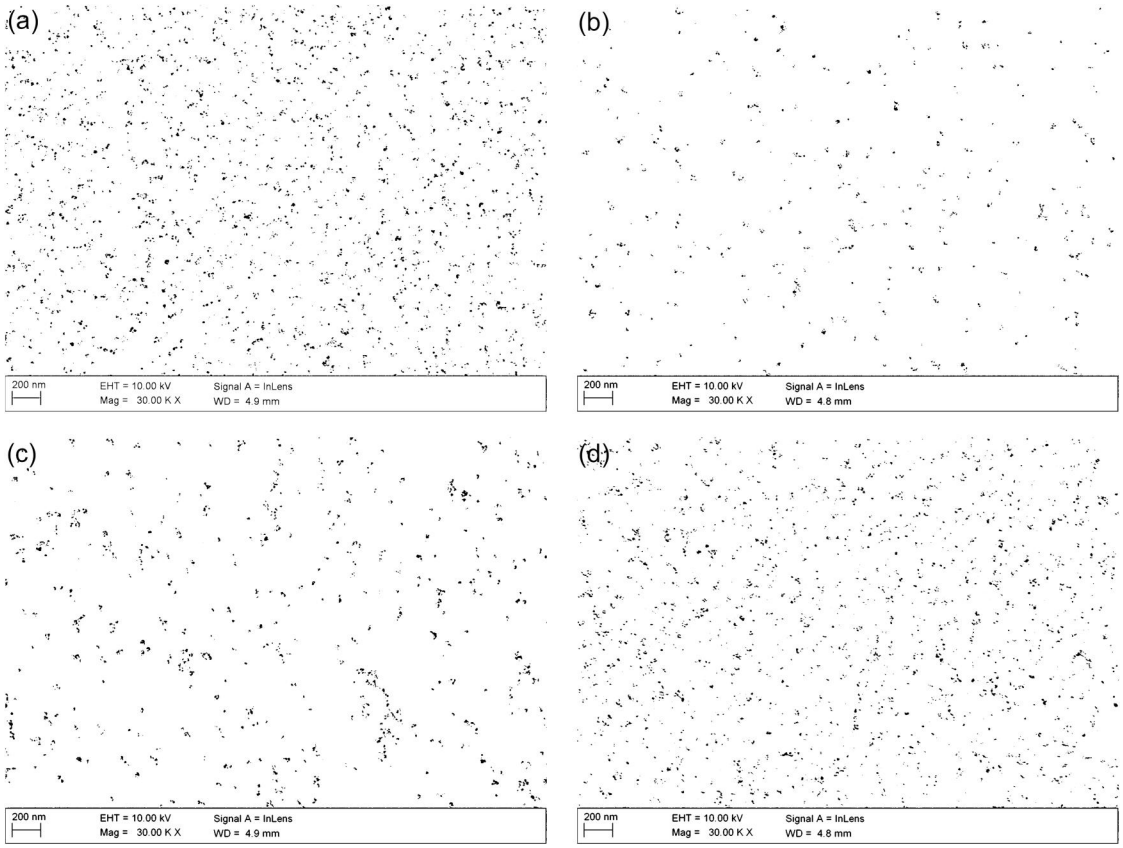

Figure 7. Field-emission scanning electron microscope (FE-SEM) images of the contaminated Si wafer (a) before and after droplet impact for 3 s, (b) at 50 m/s, (c) at 33 m/s, and (d) at 14 m/s.

region (see '$A_{overlap}$' in Figure 6b) would remain due to the difficulty of removing particles in the first annular region. As droplet impacts continue (see Figure 6c), the total clean area increases, but only to a limited extent due to the increasing overlap and the decrease in untouched region. Consequently, we could aggregate newly-created clean areas over a cleaning time duration to predict the particle removal efficiency (PRE), which is defined as the ratio of the total clean area to the original surface area of wafer ($A_{wafer} = 1\,cm^2$).

Understanding various characteristic times is crucial for assessing the validity of assumptions used in our MC modeling. According to Park et al. (2024), particles within $r \leq D_R/2$ apparently migrate toward the annular region after detaching from the surface and eventually resettle on it during their single-droplet experiment. We defined the resettlement time of detached particles as $\tau_{rs} = 18\eta_l h_m / g d_p^2 (\rho_p - \rho_l)$, where ρ_p and ρ_l are the densities of the particle and liquid, η_l is the liquid viscosity, h_m is the thickness of the liquid film at $r = D_{max}/2$, and g is the gravitational acceleration. For instance, upon the impact of a single 23-μm water droplet at $U = 14$ m/s, CFD simulations indicated $h_m \geq 5.6\,\mu m$, resulting in $\tau_{rs} \geq 33.2$ s for titanium particles of 130 nm, given properties $\rho_p = 4540\,kg/m^3$, $\rho_l = 997\,kg/m^3$, and $\eta_l = 8.89 \times 10^{-4}$ Pa·s. Recalling Figure 5, the wafer surface was fully covered with a continuous water film at $\tau_{film} = 2.3$ s, which is much shorter than the τ_{rs} even at the lowest impact velocity ($U = 14$ m/s). This suggests that once detached, particles are carried away from the surface by the water flow before resettling. Another significant time is the time interval between successive droplet impacts (τ_{int}). Given a liquid volume flow rate (Q_l), a spray divergent angle (θ), an average droplet diameter ($\overline{D}_0$), and a nozzle-to-wafer distance (h), the impaction rate of droplets onto the wafer is calculated as $\dot{N}_{wafer} = \frac{6Q_l}{\pi \overline{D}_0^3} \frac{A_{wafer}}{A_{spray}}$, where A_{spray} represents the cross-sectional area of the spray at distance h, given by $A_{spray} = \pi(h \cdot tan(\theta/2))^2$. Thus, τ_{int} is calculated as $\tau_{int} = 1/\dot{N}_{wafer}$, resulting in $\tau_{int} = 7.3\,\mu s$ at $U = 14$ m/s ($h = 150$ mm), $\theta = 27°$, $\overline{D}_0 = 23.4\,\mu m$, and $Q_l = 10$ ccm. Our CFD simulations (Park et al. 2024) confirmed that the time (τ_{sp}) for a droplet to fully spread and reach D_{max} is approximately 6.6 μs under the same condition, which is shorter than τ_{int}. This indicates that a single droplet fully spreads before the

impact of the next droplet, validating the sequential sampling approach of droplets in our MC model. Furthermore, the times τ_{int} and τ_{film} are too short to allow significant evaporation of water traces. This suggests that particles in the annular region are protected from any subsequent droplet impacts by the cushioning effect of the remaining water film (Kondo and Ando 2019).

3. Results and discussion

3.1. Experimental validation for PRE predictions of MC model

Following the procedure described in Section 2.2, we conducted experiments to measure particle removal efficiencies at different impact velocities of droplets and used the results to validate the model predictions of PRE. Figure 7 shows the FE-SEM images of the wafer surface before and after droplet impacts at three different velocities over a duration of 3 s. Figure 7a visualizes the wafer surface contaminated with Ti nanoparticles prior to droplet impacts, where the particles appear to be randomly distributed on the surface. In contrast, Figures 7b–d show particles remaining after cleaning at droplet velocities of 50, 33, and 14 m/s, respectively. Clearly, the number of particles gradually decreases with increasing droplet velocity. It is also important to note that those particles in Figures 7b–d are not significantly different from those seen in Figure 7a and remain spatially distributed randomly on the surface, without forming circular clusters even after cleaning. The absence of water marks is likely attributed to our post-treatment of cleaned wafers with isopropanol (refer to Section 2.2).

We conducted image analysis on the images in Figure 7 to determine the size distribution of particles present in each case. Figure 8 compares the particle size distributions corresponding to Figures 7a–d. The vertical axis represents the number of particles within each size bin, normalized by the image area, while the error bars indicate the standard deviations of the particle number density for each size. Notably, the small error bars suggest that the sizes and counts of existing particles are consistent across the entire wafer surface. When comparing the size distributions obtained before and after cleaning at $U = 14$ m/s (see squares and circles in Figure 8), it is evident that smaller particles are more difficult to remove, consistent with previous reports (Park et al. 2024; Sato et al. 2011; Snow, Sato, and Tanaka 2013). For example, 15-nm particles show approximately a 27% decrease in their number density, from 46 to 34 #/μm^2, while 50-nm

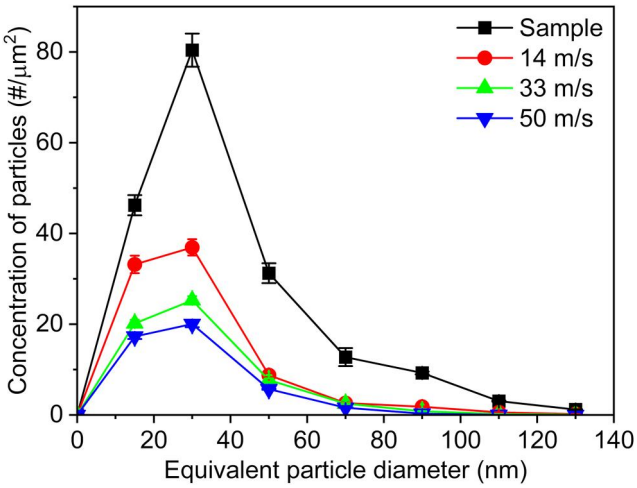

Figure 8. Comparison of the number size distributions of particles remaining on the wafer surface before and after cleaning at three different droplet velocities.

particles exhibit a 68% decrease. Particles larger than 90 nm seem to be almost completely removed by the 3-s cleaning. Higher-velocity droplet impacts, such as those at 33 m/s, are observed to be more effective at removing smaller particles, particularly in the 15-to-30 nm range. However, further increasing the droplet velocity to 50 m/s does not yield additional benefits, suggesting that this may be near the upper limit of cleaning efficiency for the 3-s cleaning.

The difference in particle number density before and after cleaning ($N_{before} - N_{after}$) at each size was normalized by the value before cleaning (N_{before}) to calculate the particle removal efficiency (PRE) by particle size. In addition, we conducted similar cleaning experiments with shorter cleaning times of 1 and 2 s at each droplet impact velocity. Figure 9a compares the size-resolved PRE profiles experimentally obtained at $U = 14$ m/s with those predicted by the MC model for three distinct cleaning times. Notably, the MC model's prediction for the 1-s cleaning time is nearly perfect. For the 2- and 3-s cleaning times, the model tends to slightly underpredict the PREs of 15–30 nm particles and overpredict those of particles larger than 90 nm. Despite these minor discrepancies, the MC model accurately predicts the change in PRE with increasing the cleaning time across the entire particle size range. For instance, increasing the cleaning time to 2 s is recommended for improving PRE, while further increases in cleaning time yield only small gains in PRE, consistent with experimental observations.

Figure 9b and c compare the PRE profiles between the model predictions and experimental data for droplet impacts at elevated velocities of 33 m/s and 50 m/s, respectively. Unlike Figure 9a, the three different

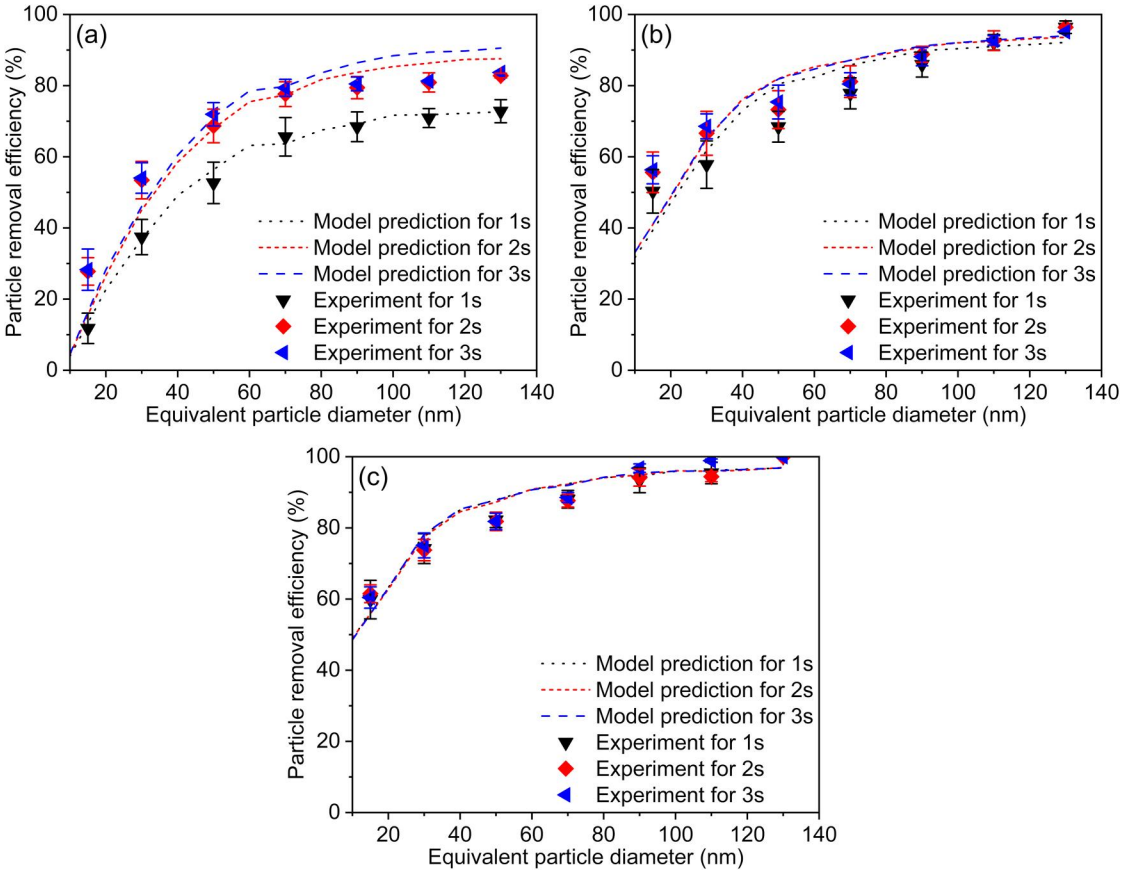

Figure 9. Comparison of size-resolved PRE profiles obtained from the experiments and MC model predictions for three different cleaning times under droplet impacts at (a) 14 m/s, (b) 33 m/s, and (c) 50 m/s.

symbols or lines in these figures tend to converge into a single trend. This represents that both the experiment and the MC model indicate that the cleaning time of 1 to 3 s is no longer a control parameter for the PRE under high-velocity droplet impacts. In other words, a cleaning time of 1 s, for example, at $U =$ 50 m/s is likely sufficient for our spray cleaning process to reach an upper limit in PRE. Examining Figures 9b and a closely, it becomes apparent that the time required to reach the upper limit of cleaning seems to increase to between 1 and 2 s at $U = 33$ m/s and between 2 and 3 s at $U = 14$ m/s. Interestingly, this time correlates well with the time for water film formation (τ_{film}) discussed in Section 2.2, where $\tau_{film} = 0.4$, 1.3, and 2.3 s for $U = 50$ m/s, 33 m/s, and 14 m/s, respectively. This correlation further supports the adverse effect of liquid film formation on spray cleaning, as a result of the cushioning effect mentioned earlier. Notably, only 1 s (or less) of spray cleaning at a velocity of 50 m/s can achieve a PRE of $\geq$ 80% for particles larger than 50 nm, surpassing the limitations of cleaning time and PRE reported in previous studies listed in Table 1. However, even at the highest impact velocity, the PRE is still as low as 61% for 15-nm particles in Figure 9c, which may be insufficient for industrial applications.

3.2. Further improvement of jet spray cleaning

This section describes our efforts to further improve particle removal efficiencies (PREs), particularly for 15–30 nm particles which have not been tested to date. As discussed earlier, continuous cleaning methods encounters a critical limitation in PRE due to the cushioning effect created when a water film covers the wafer surface. Since the current limitation stems from the presence of a water film, our key idea began with a simple question: What would happen if we removed the water film (created during the first cleaning) and conducted the second cleaning on the dried wafer surface? To test this, we divided the 3-s continuous spray cleaning process into n cycles of a combined subprocess of spray cleaning and drying. Specifically, we established a 1-s spray cleaning at $U = 50$ m/s followed by a 20-second drying as a unit subprocess, and repeated this 1 to 3 times. For the drying process, we injected only nitrogen gas at 50 lpm through the same nozzle. We

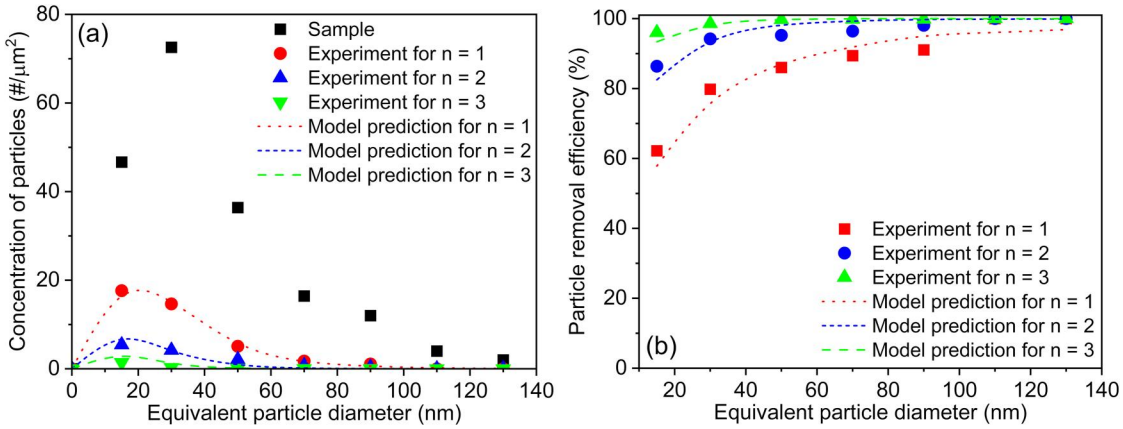

Figure 10. Comparison of (a) size distributions and (b) PRE profiles of particles remaining after n cycles of spray cleaning between experimental data and model predictions, under droplet impacts at 50 m/s.

also attempted to predict PREs as a function of particle diameter (d_p) after n cycles as follows: (1) Start with the size-resolved PRE data predicted by our MC model for 1-s spray cleaning (see the black dotted line in Figure 9c) as $PRE(d_p)$; (2) Calculate the number density of particles remaining after n cycles, $N_n(d_p)$, using the definition of PRE and the number density of pristine particles $N_0(d_p)$ (see 'sample' in Figure 8) as $N_n(d_p) = N_0(d_p)(1 - PRE(d_p))^n$; (3) Calculate the overall PRE data after n cycles as $PRE_n(d_p) = 1 - (1 - PRE(d_p))^n$.

Figure 10a presents the size distribution of particles remaining after n cycles ($N_n(d_p)$), in comparison to $N_0(d_p)$. Symbols represent experimental data, while dotted lines represent predictions from the MC model. It is important to note that the repeated spraying and drying of droplets effectively remove particles across the entire size range. In particular, 15-nm particles are continuously removed with each cleaning cycle, eventually reducing their number density to 2.7 #/μm^2 after the third cycle. Additionally, the predicted size distribution, $N_n(d_p)$, closely matches the experimental data for each cycle. Based on the experimental data for $N_n(d_p)$ in Figure 10a, we estimated $PRE_n(d_p)$ for each cycle and compared these experimental estimates to the predictions given by the equation for $PRE_n(d_p)$, as shown in Figure 10b. The model once again provides reasonable predictions of PRE values across particle size range, regardless of the cycle number. As expected, the cleaning efficiency (PRE_n) for 15-nm particles continuously improves with each cycle: 61% after the first cycle, 87% after the second, and 94% after the third. To our knowledge, this is the first experimental demonstration of near-complete removal of 15-nm particles within 1 min.

Until now, we have shown that the promising results can be reasonably predicted by our MC model, which is applicable to the removal of *spherical* particles. Revisiting Figures 7 and S1a, one might raise concerns about the potential agglomeration of particles that may affect the prediction accuracy of the model. According to Tran-Cong, Gay, and Michaelides (2004), the drag coefficients for irregular particles (C_{DA}) can be well approximated by Stokes law ($C_{DA} \approx 24/Re_A$), regardless of the actual shapes of the particles, when their Reynolds number ($Re_A = \rho_l V_R d_A/\eta_l$) is smaller than 1.0. Here, d_A is the projected area-equivalent diameter of the irregular particles. Since $Re_A < 1$ in this study, their result leads to two notable scaling relations: $C_{DA} \propto 1/d_A$ and $F_{DA} = C_{DA}\pi d_A^2 \rho_l V_R^2/8 \propto d_A$ for a constant local velocity (V_R). These relations suggest that the projected area of agglomerated particles becomes the most influential factor in determining the drag force (F_{DA}). For this reason, we plotted the size distributions of particles before and after cleaning, as well as the resulting PREs, as a function of d_A in Figures 8–10. Interestingly, in the figures, the MC model reasonably predicts the variations of PREs, regardless of particle agglomeration, by utilizing d_A in place of d_p in Equation (1).

It is also interesting to recall the finding in Figure S1: while some particles are agglomerated, they were few in number and significantly larger than the size range of primary interest in this study (10–30 nm, as stated in Introduction). Therefore, our MC model predictions are valid, at least within the 10–60 nm size range, where particles are predominantly non-agglomerated. Moreover, Figures 9 and 10 show that PREs predicted exhibit the significant changes within the size range, highlighting the key characteristics of the current particle removal process. Thus, we conclude that the potential impact of particle agglomeration is minimal in this study.

4. Conclusion

In this study, we proposed two novel approaches to overcome the technical limitations associated with removing contaminant particles in the 10–30 nm range from Si wafers using a liquid jet spray. First, we developed a Monte Carlo model to address the lack of predictive models for particle removal efficiency in real-world cleaning experiments. This MC model was successfully validated through a series of cleaning experiments for 10–130 nm particles on Si wafer surface, using on a two-fluid supersonic nozzle that controlled impact velocities of sprayed microdroplets. Both the model and experiments consistently revealed notable characteristics of PRE profiles by particle size, including that smaller particles are more challenging to remove than larger ones. More importantly, we demonstrated for the first time the significance of cleaning time duration, showing that continued droplet spray after the formation of a liquid film on the surface has a negligible effect on PREs. To minimize the adverse effects of liquid film formation, we proposed a cyclic repetition of spraying droplets and drying the surface as the second trial, which resulted in a dramatic increase in PREs, particularly for the removal of 10–30 nm particles. Specifically, for 15-nm particles, when droplets were sprayed continuously for 3 s at a velocity of 50 m/s, the PRE was as low as 61%. However, when droplets were sprayed for 1 s, followed by a 20-second drying process in one cycle, and this process was repeated three times, the PRE for 15-nm particles eventually increased to 94%. This result strongly supports that liquid jet spray cleaning can be an effective solution to meet the recent demand for removing smaller contaminant particles from wafer surfaces in the semiconductor industry.

Nomenclature

a	radius of contact between a particle and the Si wafer surface
$A_{overlap}$	overlapped region due to subsequent droplet impacts
A_{remain}	region where particles remain unaffected by further spreading of liquid
A_{spray}	cross-sectional area of droplet spray
A_{wafer}	area of the Si wafer
C_{DA}	drag coefficient for an agglomerated particle
d_A	projected-area equivalent diameter of the agglomerated particle
d_p	diameter of a spherical particle
D_0	initial droplet diameter before impact
$\overline{D}_0$	average droplet diameter
D_R	effective cleaning diameter of a droplet on the surface
D_{max}	maximum spreading diameter of a droplet on the surface
F_{ad}	adhesion force between a particle and the surface
F_D	drag force exerted on an attached spherical particle by a spreading liquid film
F_{DA}	drag force exerted on an agglomerated particle
F_L	lift force exerted on the particle in a spreading liquid
g	gravitational acceleration
h	distance from the nozzle exit to the wafer surface
h_{film}	thickness of liquid film when the surface is completely covered
h_m	thickness of liquid film at its maximum spreading
m	mass of liquid on the wafer
M_D	rotational moment induced by surface stress on particle surface
n	number of cleaning cycle
N	number of existing particles on the surface
$\dot{N}_{wafer}$	impaction rate of droplets
Q_g	volume flow rate of gas through the nozzle
Q_l	volume flow rate of ultrapure water through the nozzle
r	radius from the point of impact
Re_A	Reynolds number based on the local velocity and projected area equivalent diameter
U	impact velocity of a droplet
V_R	local flow velocity of spreading liquid at the location of particle center

Greek symbols

η_l	liquid viscosity
θ	spray divergent angle
ρ_l	density of liquid
ρ_p	density of particle
τ_{film}	time required until the surface is completely covered
τ_{int}	time interval between two consecutive droplet impacts
τ_{rs}	time for complete resettlement of detached particles in the liquid film
τ_{sp}	time for the spreading liquid film to reach D_{max}

Note that all variables are expressed in SI units unless otherwise stated.

Disclosure statement

No potential conflict of interest was reported by the author(s).

Funding

This research was supported by Basic Science Research Program through the National Research Foundation of Korea (NRF) funded by the Ministry of Education [No. 2020R1A2C2011634] and also by the Ministry of Trade, Industry and Energy (MOTIE) and Korea Institute for Advancement of Technology (KIAT) through the International Cooperative R&D program [Project No. P0027902].

References

Banerjee, S., and A. Campbell. 2005. Principles and mechanisms of sub-micrometer particle removal by CO_2 cryogenic technique. *J. Adhes. Sci. Technol.* 19 (9):739–51. doi:10.1163/1568561054867828.

Burdick, G., N. Berman, and S. Beaudoin. 2001. Describing hydrodynamic particle removal from surfaces using the particle reynolds number. *Journal of Nanoparticle Research* 3 (5/6):453–65. doi:10.1023/A:1012593318108.

Castanet, G., P. Dunand, O. Caballina, and F. Lemoine. 2013. High-speed shadow imagery to characterize the size and velocity of the secondary droplets produced by drop impacts onto a heated surface. *Exp. Fluids* 54 (3):1489. doi:10.1007/s00348-013-1489-3.

Choudhury, R., J. Choi, S. Yang, Y.-J. Kim, and D. Lee. 2017. Maximum spreading of liquid drop on various substrates with different wettabilities. *Appl. Surf. Sci.* 415: 149–54. doi:10.1016/j.apsusc.2016.12.195.

Eigel, J. D., and I. D. Moore. 1983. A simplified technique for measuring raindrop size and distribution. *Transactions of the ASAE* 26(4):1079–1084. doi:10.13031/2013.34080.

Eitoku, A., R. Vos, J. Snow, M. Sato, S. Hirae, K. Nakajima, M. Nonomura, M. Imai, P. W. Mertens, and M. M. Heyns. 2003. Removal of small (<100-nm) particles and metal contamination in single-wafer cleaning tool. *SSP.* 92:157–60. doi:10.4028/www.scientific.net/SSP.92.157.

Eranna, G. 2014. *Crystal Growth and Evaluation of Silicon for VLSI and ULSI, 347-77*. Boca Raton, FL: CRC Press. doi:10.1201/b17812.

Hattori, T., H. Hirano, T. Osaka, and H. Kuniyasu. 2007. Environmentally benign single-wafer spin cleaning using ultra-diluted HF/nitrogen jet spray without causing structural damage and material loss. *IEEE Trans. Semicond. Manufact.* 20 (3):252–8. doi:10.1109/TSM.2007.901845.

Hirano, H., K. Sato, T. Osaka, H. Kuniyasu, and T. Hattori. 2006. Damage-free ultradiluted HF/nitrogen jet spray cleaning for particle removal with minimal silicon and oxide loss. *Electrochem. Solid-State Lett.* 9 (2):G62–G65. doi:10.1149/1.2153857.

Hirota, Y., I. Kanno, K. Fujiwara, H. Nagayasu, and S. Shimose. 2005. Damage-free wafer cleaning by water and gas mixture jet. In IEEE International Symposium on Semiconductor Manufacturing, 219–22. doi:10.1109/ISSM.2005.1513340.

Hong, J., X. Niu, Y. Liu, Y. He, B. Zhang, J. Wang, L. Han, C. Yan, and J. Zhang. 2016. Effect of a novel chelating agent on defect removal during post-CMP cleaning. *Appl. Surf. Sci.* 378:239–44. doi:10.1016/j.apsusc.2016.03.230.

Huang, Y., D. Guo, X. Lu, and J. Luo. 2011. Mechanisms for nanoparticle removal in brush scrubber cleaning. *Appl. Surf. Sci.* 257 (7):3055–62. doi:10.1016/j.apsusc.2010.10.115.

Institute of Electrical and Electronics Engineers. 2023. IEEE International Roadmap for Devices and *Systems: Systems and Architectures*. doi:10.60627/JC06-2E45.

Iwasaki, A., A. Higuchi, K. Komori, M. Sato, and H. Shirakawa. 2015. Dual-fluid spray process for particle and fluorocarbon-polymer removal in BEOL applications. *ECS Trans.* 69 (8):199–205. doi:10.1149/06908.0199ecst.

Ji, H., C. Mi, Z. Yuan, Y. Liu, H. Zhu, and F. Meng. 2022. Multicomponent gas detection method via dynamic temperature modulation measurements based on semiconductor gas sensor. *IEEE Trans. Ind. Electron.* 70 (6): 6395–404. doi:10.1109/TIE.2022.3194629.

Kern, W. 1990. The evolution of silicon wafer cleaning technology. *J. Electrochem. Soc.* 137 (6):1887–92. doi:10.1149/1.2086825.

Kim, B. S., T. W. Koo, J. H. Lee, D. S. Kim, Y. C. Jung, S. W. Hwang, B. L. Choi, E. K. Lee, J. M. Kim, and D. M. Whang. 2009. Catalyst-Free Growth of Single-Crystal Silicon and Germanium Nanowires. *Nano Lett.* 9 (2):864–9. doi:10.1021/nl803752w.

Kim, J., and D. Lee. 2023. Evolution of pore structure in nanoparticle deposits from unimodal to bimodal pore size distributions: Focus on structural features of dendritic structures. *J. Aerosol Sci.* 173:106227. doi:10.1016/j.jaerosci.2023.106227.

Kim, J., J. Shin, and D. Lee. 2022. Microstructural transition of nanoparticle deposits from multiple dendrites to compact layer. *J. Aerosol Sci.* 159:105876. doi:10.1016/j.jaerosci.2021.105876.

Kondo, T., and K. Ando. 2019. Simulation of high-speed droplet impact against a dry/wet rigid wall for understanding the mechanism of liquid jet cleaning. *Phys. Fluids.* 31 (1):013303. doi:10.1063/1.5079282.

Kurumoto, N., A. Eitoku, and K. Miya. 2009. Relationship between atmospheric humidity and watermark formation in IPA dry of Si wafer after HF clean. *SSP.* 145-146:91–4. doi:10.4028/www.scientific.net/SSP.145-146.91.

Lee, J. H., H. Y. Ryu, J. K. Hwang, N. P. Yerriboina, T. G. Kim, S. Hamada, Y. Wada, H. Hiyama, and J.-G. Park. 2019. A breakthrough method for the effective conditioning of PVA brush used for post-CMP process. *ECS J. Solid State Sci. Technol.* 8 (6):P307–P312. doi:10.1149/2.0111906jss.

Lee, H., S. You, P. V. Pikhitsa, J. Kim, S. Kwon, C. G. Woo, and M. Choi. 2011. Three-dimensional assembly of nanoparticles from charged aerosols. *Nano Lett.* 11 (1):119–24. doi:10.1021/nl103787k.

Leite, F. L., C. C. Bueno, A. L. Da Róz, E. C. Ziemath, and O. N. Oliveira. 2012. Theoretical models for surface forces and adhesion and their measurement using atomic force microscopy. *Int. J. Mol. Sci.* 13 (10):12773–856. doi:10.3390/ijms131012773.

Liu, L. H., and B. L. Liu. 2011. Research of ice jet cleaning surface. *AMR.* 233–235:777–84. doi:10.4028/www.scientific.net/AMR.233-235.777.

Liu, Q., H. E. Ruda, G. M. Chen, and M. Simard-Normandin. 1996. A generalized approach to surface photovoltage. *J. Appl. Phys.* 79 (10):7790–9. doi:10.1063/1.362386.

Ock, Y., J. Kim, I. Choi, D. S. Kim, M. Choi, and D. Lee. 2018. Size-independent unipolar charging of nanoparticles at high concentrations using vapor condensation and its application for improving DMA size-selection efficiency. *J. Aerosol Sci.* 121:38–53. doi:10.1016/j.jaerosci.2018.04.007.

Ohmi, T., M. Miyashita, M. Itano, T. Imaoka, and I. Kawanabe. 1992. Dependence of thin-oxide films quality on surface microroughness. *IEEE Trans. Electron Devices* 39 (3):537–45. doi:10.1109/16.123475.

Park, J., S. Lee, J. Kim, and D. Lee. 2024. Capability and efficiency of droplets in removing nanoparticle contaminants from Si wafer via high-speed microdroplet

impaction. *Aerosol Sci. Technol.* 58 (9):1008–23. doi:10.1080/02786826.2024.2338523.

Reinhardt, K., and W. Kern. 2018. *Handbook of silicon wafer cleaning technology: Section I: Introduction and Overview*. Norwich, NY: William Andrew Publishing. doi:10.1016/B978-0-323-51084-4.00001-0.

Sato, M., K. Sotoku, K. Yamaguchi, T. Tanaka, M. Kobayashi, and S. Nadahara. 2011. Analysis on threshold energy of particle removal in spray cleaning technology. *ECS Trans.* 41 (5):75–82. doi:10.1149/1.3630829.

Seike, Y., K. Miyachi, T. Shibata, Y. Kobayashi, S. Kurokawa, and T. Doi. 2010. Silicon wafer cleaning using new liquid aerosol with controlled droplet velocity and size by rotary atomizer method. *Jpn. J. Appl. Phys.* 49 (6R):066701. doi:10.1143/JJAP.49.066701.

Snow, J. T., M. Sato, and T. Tanaka. 2013. Developments in surface contamination and cleaning. In *Dual-Fluid Spray Cleaning Technique for Particle Removal*, ed. R. Kohli and K. L. Mittal, 107. Oxford, UK: Elsevier. doi:10.1016/B978-1-4377-7879-3.00003-0.

Teng, Y., H. Cui, X. He, J. Li, J. Han, Q. Jiang, X. Liu, C. Zhao, and Y. Wu. 2016. Damage free removal of nanoparticles with dual-fluid spray nozzle cleaning. In China Semiconductor Technology International Conference (CSTIC) 2016, 1–3. doi:10.1109/CSTIC.2016.7463993.

Toscano, C., and G. Ahmadi. 2003. Particle removal mechanisms in cryogenic surface cleaning. *The Journal of Adhesion* 79 (2):175–201. doi:10.1080/00218460309570.

Tran-Cong, S., M. Gay, and E. E. Michaelides. 2004. Drag coefficients of irregularly shaped particles. *Powder Technol.* 139 (1):21–32. doi:10.1016/j.powtec.2003.10.002.

Watanabe, M., T. Sanada, A. Hayashida, and Y. Isago. 2009. Cleaning technique using high-speed steam-water mixed spray. *SSP.* 145-146:43–6. doi:10.4028/www.scientific.net/SSP.145-146.43.

Xu, K., S. Pichler, K. Wostyn, G. Cado, C. Springer, G. W. Gale, M. Dalmer, P. W. Mertens, T. Bearda, E. Gaulhofer, et al. 2009. Removal of nano-particles by aerosol spray: Effect of droplet size and velocity on cleaning performance. *SSP.* 145-146:31–4. doi:10.4028/www.scientific.net/SSP.145-146.31.

Zantye, P. B., A. Kumar, and A. K. Sikder. 2004. Chemical mechanical planarization for microelectronics applications. *Mat. Sci. Eng.* 45 (3–6):89–220. doi:10.1016/j.mser.2004.06.002.

Zoeteweij, M. L., J. C. J. van der Donck, and R. Versluis. 2009. Particle removal in linear shear flow: Model prediction and experimental validation. *J. Adhes. Sci. Technol.* 23 (6):899–911. doi:10.1163/156856109X411247.